Anthropogenic influences on the extremely dry and hot summer of 2020 in Southern China and projected changes in the likelihood of the event

Weather and Climate Extremes 45 (2024) 100706

Contents lists available at ScienceDirect

Weather and Climate Extremes

journal homepage: www.elsevier.com/locate/wace

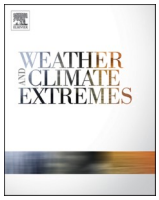

Anthropogenic influences on the extremely dry and hot summer of 2020 in Southern China and projected changes in the likelihood of the event

Kaixi Wang [a], Zhiyuan Zheng [b,l,m,*], Xian Zhu [a,m], Wenjie Dong [a,m], Simon F.B. Tett [c], Buwen Dong [d], Wenxia Zhang [e], Fraser C. Lott [f], Lulei Bu [g], Yumiao Wang [h], Huixin Li [i], Nergui Nanding [j], Nicolas Freychet [c], Dongqian Wang [k], Shaobo Qiao [a,m]

[a] School of Atmospheric Sciences, Key Laboratory of Tropical Atmosphere-Ocean System (Sun Yat-sen University), Ministry of Education, Sun Yat-sen University, Zhuhai, China
[b] Zhuhai Branch of State Key Laboratory of Earth Surface Process and Resource Ecology, Advanced Institute of Natural Sciences, Beijing Normal University, Zhuhai, China
[c] School of Geosciences, University of Edinburgh, Edinburgh, UK
[d] National Centre for Atmospheric Science, Department of Meteorology, University of Reading, Reading, UK
[e] State Key Laboratory of Numerical Modeling for Atmospheric Sciences and Geophysical Fluid Dynamics, Institute of Atmospheric Physics, Chinese Academy of Sciences, Beijing, China
[f] Met Office Hadley Centre, Exeter, EX1 3PB, UK
[g] Department of Atmospheric and Oceanic Sciences & Institute of Atmospheric Sciences, IRDR International Center of Excellence on Risk Interconnectivity and Governance on Weather/Climate Extremes Impact and Public Health, Fudan University, Shanghai, China
[h] School of Hydrology and Water Resources, Nanjing University of Information Science and Technology, Nanjing, China
[i] Collaborative Innovation Center on Forecast and Evaluation of Meteorological Disasters/Key Laboratory of Meteorological Disasters, Ministry of Education/Joint International Research Laboratory of Climate and Environment Change, Nanjing University of Information Science and Technology, Nanjing, China
[j] School of Earth Sciences, Yunnan University, Kunming, China
[k] National Climate Center, China Meteorological Administration, Beijing, China
[l] State Key Laboratory of Earth Surface Processes and Resource Ecology, Faculty of Geographical Science, Beijing Normal University, Beijing, China
[m] Southern Marine Science and Engineering Guangdong Laboratory (Zhuhai), Zhuhai, China

ARTICLE INFO

Keywords:
Extremely dry and hot summer
Anthropogenic influences
Projection
Southern China

ABSTRACT

During summer 2020, Southern China experienced an extremely dry and hot summer, which was identified as one of the top ten domestic weather and climate extreme events in 2020 by China Meteorological Administration. Summer mean precipitation, surface air temperature (TAS), and number of hot days (NHD) were about 25% dryer, 1.5 °C warmer, and 11 days larger than the 1981–2010 climatologies. These are the 4th largest precipitation deficit, the highest TAS, and the 2nd highest NHD in the 1961–2020 record. The large-scale circulation anomalies over the West Pacific increased the likelihood of the extreme hot and dry summer. Anthropogenic influences on this extreme summerwere investigated using 525-member ensembles of the atmosphere-only HadGEM3-GA6 model and the multi-model ensembles from the Coupled Model Intercomparison Project Phase 6 (CMIP6). Anthropogenic forcings doubled (increased by 27%) the probability of precipitation deficits, and increased occurrence more than 10^6 times for both TAS anomaly (50 times probability higher) and NHD anomaly (6 times probability higher) in HadGEM-GA6 (CMIP6). That means that the 2020-like TAS and NHD anomalies would not occur without anthropogenic forcings, and there is weak evidence that human influences decrease rainfall over Southern China. However, the precipitation deficit increased the likelihood of exceeding the observed thresholds for both TAS and NHD by about 17 (4) and 9 (1) times in HadGEM3-GA6 (CMIP6), respectively. Under SSP2-4.5 and SSP5-8.5 scenarios in the future, 2020-like hot but wet extreme summer increases in magnitude and frequency, while the frequency of dry summer declines.

* Corresponding author. Zhuhai Branch of State Key Laboratory of Earth Surface Process and Resource Ecology, Advanced Institute of Natural Sciences, Beijing Normal University, Zhuhai 519087, China.
E-mail address: zhiyzheng@bnu.edu.cn (Z. Zheng).

https://doi.org/10.1016/j.wace.2024.100706
Received 17 November 2023; Received in revised form 30 May 2024; Accepted 17 June 2024
Available online 19 June 2024

Table 1
List of CMIP6 models and their members used in this study.

No.	Model name	Modeling center (or group)	Historical	Hist-nat	SSP2-45	SSP5-85	Spatial resolution (# of Lon × # of Lat)
1	ACCESS-CM2	Commonwealth Scientific and Industrial Research Organisation, Australia	5	3	5	5	192 × 144
2	ACCESS-ESM1-5	Commonwealth Scientific and Industrial Research Organisation, Australia	40	3	40	40	192 × 145
3	BCC-CSM2-MR	Beijing Climate Center, China Meteorological Administration, China	1	3	1	1	320 × 160
4	CanESM5	Canadian Centre for Climate Modelling and Analysis, Environment and Climate Change Canada, Canada	25	25	25	25	128 × 64
5	CNRM-CM6-1	Centre National de Recherches Météorologiques, France	6	10	6	6	265 × 128
6	FGOALS-g3	LASG, Institute of Atmospheric Physics, Chinese Academy of Sciences, China	4	3	4	4	180 × 80
7	GFDL-ESM4	National Oceanic and Atmospheric Administration, Geophysical Fluid Dynamics Laboratory, United States	3	3	3	1	288 × 180
8	HadGEM2-GC31-LL	Met Office Hadley Centre, United Kingdom	5	10	5	4	180 × 120
9	IPSL-CM6A-LR	Institution Pierre Simon Laplace, France	11	10	11	6	144 × 143
10	MIROC6	Japan Agency for Marine-Earth Science and Technology, Japan	50	10	50	10	256 × 128
11	MRI-ESM2-0	Meteorological Research Institute, Japan	5	5	5	5	320 × 160
12	NorESM2-LM	NorESM Climate modeling Consortium consisting of Center for International Climate and Environmental Research, Norway	3	3	3	1	144 × 96

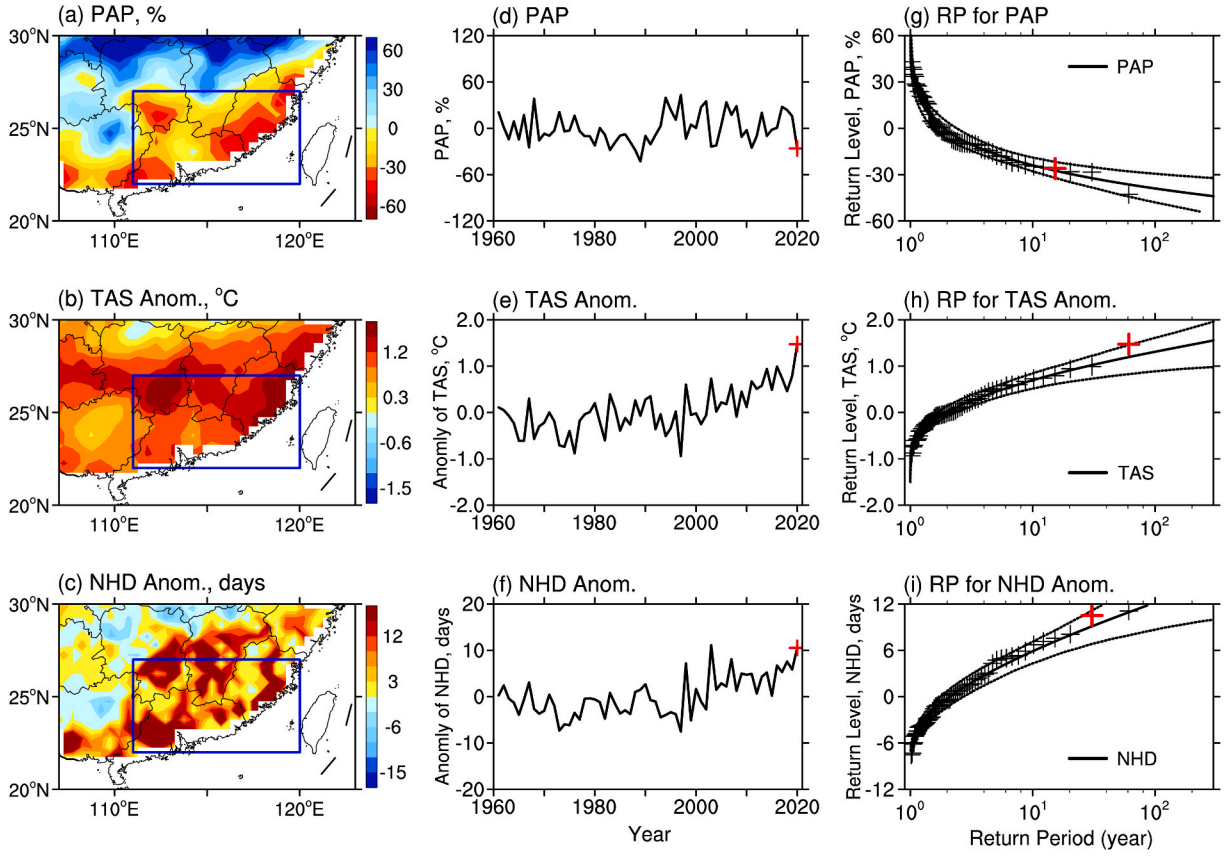

Fig. 1. Spatial patterns of (a) percentage of anomalous precipitation (PAP; %), (b) surface air temperature (TAS; °C), and (c) the number of hot days (NHD; day) anomalies in June–August 2020 relative to 1981–2010. Timeseries of observed (black; 1961–2020) June–August (d) PAP, (e) TAS, and (f) NHD anomalies, regionally averaged in Southern China [blue boxes in a–c], where red crosses denote 2020. Return periods and 95% confidence intervals for June–August (g) PAP, (h) TAS, and (i) NHD anomalies. The black dashed lines denote the 2.5th–97.5th percentile uncertainty range where red crosses denote the year 2020. (For interpretation of the references to colour in this figure legend, the reader is referred to the Web version of this article.)

1. Introduction

Southern China is located in the subtropical and tropical monsoon climate zone with more than 1 500 mm of precipitation per year, making it one of the most humid and rainy areas in China (Yang et al., 2010; Li et al., 2012; Wang et al., 2018; Zheng et al., 2024). Recently, water resource issues become more sensitive and severe in this region due to enhanced drought and increased water usage from rapid urbanization (Shen et al., 2002; Kumar et al., 2015; Wang et al., 2018; Zhang et al., 2021). Observed trends toward more frequent and severe droughts have been noted in some wet and hot areas of China, for example, Southwest China experienced three extreme droughts during 2006–2011 (Wang et al., 2015; Wu et al., 2023; Yuan et al., 2023), and the severity of drought in the Pearl River Basin has intensified (Wang et al., 2018; Zhang et al., 2019; Xu et al., 2024), and seasonal drought events occurred more frequently in Southern China (Li et al., 2012; Wang et al.,

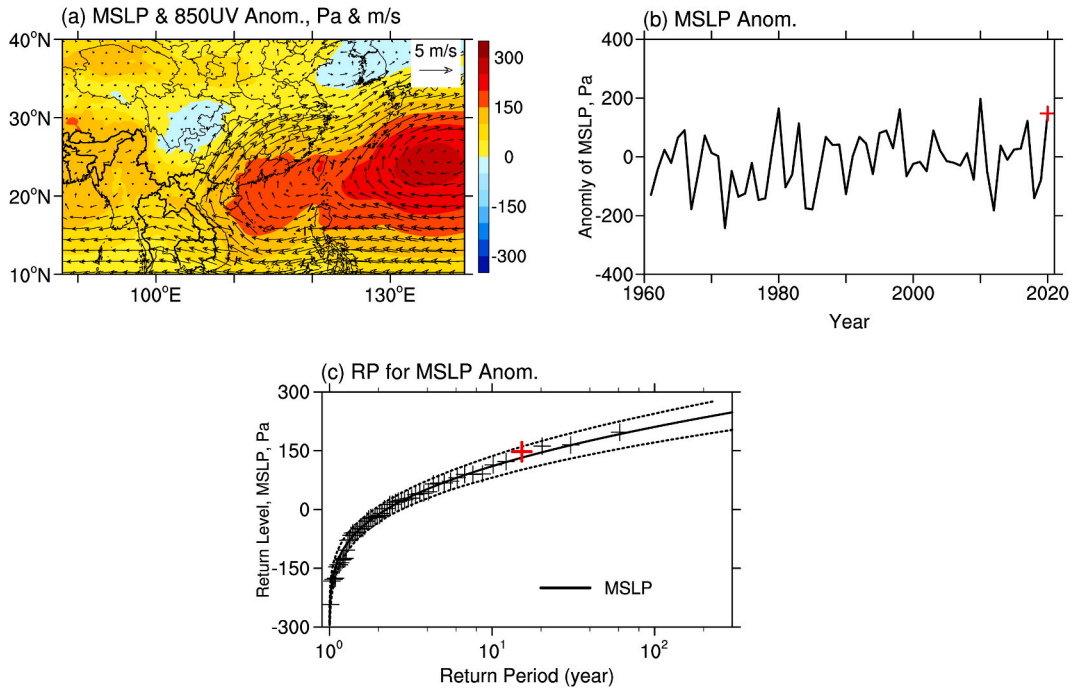

Fig. 2. (a) Spatial pattern of observed mean sea level pressure (MSLP; shading; Pa) and 850 hPa winds (vector; m s^{-1}) anomalies in June–August 2020 relative to 1981–2010 from ERA5. (b) Timeseries of observed (black; 1961–2020) June–August MSLP anomaly, regionally averaged in Southern China [blue box in Fig. 1a–c], where the red cross denotes 2020. (c) Return period and 95% confidence intervals for June–August MSLP anomaly. The black dashed lines denote the 2.5th–97.5th percentile uncertainty range where the red cross denotes the year 2020. (For interpretation of the references to colour in this figure legend, the reader is referred to the Web version of this article.)

2016; Zhang et al., 2021, 2023; Xu et al., 2023, 2024). In addition, temperature anomalies have an important role in drought intensity by amplifying evaporative demand and water loss to the atmosphere. Dry and hot events have a pronounced negative impact on the economy, resource, and ecology environment (Kumar et al., 2015; Lo et al., 2023; Wang et al., 2015; Xu et al., 2024). However, severe dry and hot summers/events occurring in humid areas are underappreciated in comparison to the sub-arid and desert regions because of their climate condition.

During summer 2020, Southern China experienced an extremely dry and hot summer affecting the provinces of Guangdong, Guangxi, Fujian, Jiangxi, and Hunan. This event was identified as one of the top ten domestic weather and climate extreme events in 2020 in China (http://www.cma.gov.cn/en2014/20150311/20200414/202101/t20210112_570009.html). China Meteorological Administration (CMA) reported that the number of hot days in Southern China was the second highest since 1961. The highest temperature recorded in Fujian (40.4 °C) was the largest since 1961. With the anomalously early end of the first annual rainy season, precipitation was less than normal over much of Southern China. The extreme rainfall deficit and abnormally high temperature contributed to shrinking reservoirs and continuous meteorological drought, increased irrigation, and water shortages in most provinces, especially in Guangxi, Guangdong and Fujian. The severe drought restricted the growth of crops such as rice and rubber. Much of Guangxi and Guangdong provinces even suffered drinking water shortages, which were rare in humid Southern China. Moreover, this extreme summer also affected transportation, power supply, and human health within Guangxi, Guangdong and Fujian provinces (https://www.cma.gov.cn/en2014/20150311/20200414/202101/t20210112_570009.html).

According to the Sixth Assessment Report of the Intergovernmental Panel on Climate Change (IPCC et al., 2021), extreme weather and climate events are both increasing in frequency and intensity in a warming world. With continuing rises in mean global temperature, many more areas around the world are suffering record-breaking extremely dry and hot events (Sun et al., 2016; Bador et al., 2017; Ma et al., 2017; Chen et al., 2019; Min et al., 2020; Devanand et al., 2023; González-Reyes et al., 2023; Holgate et al., 2023; Lo et al., 2021, 2023; Xu et al., 2023; Yuan et al., 2023; Zhang et al., 2023). Previous studies have shown that internal variability fundamentally determines whether the extreme event can happen or not, while its occurrence probability is largely influenced by anthropogenic forcings (Otto et al., 2012; Ma et al., 2017; Lo et al., 2021). Human activities have been demonstrated to contribute to recent record-breaking intense precipitation and hot events in many regions around the world (Sarojini et al., 2016; Sparrow et al., 2018; Dong et al. 2020; Min et al., 2020; Nanding et al., 2020; Li et al., 2021; IPCC et al., 2021; Yuan et al., 2023). For China, most studies show that human activities, including greenhouse gases emission, land use/cover change and urbanization, have a great impact on spring/-summer drought and heatwaves in different regions of China (Sun et al., 2016; Ma et al., 2017; Wang et al., 2016; Burke and Stott 2017; Chen et al., 2019; Ren et al., 2020; Zhang et al., 2020; Ye and Qian 2021; Zheng et al., 2022a, 2022b; Wu et al., 2023; Yuan et al., 2023). However, it is still unclear whether the attribution of anthropogenic forcings is detectable in the 2020 extremely dry and hot summer in Southern China and how the occurrence probability of similar summer will change under different future emission scenarios.

In this study, we investigate how anthropogenic forcing has changed the probability of the persistently dry and hot summer that impacted Southern China in 2020. We aim to answer the following questions: (1) What are the characteristics of the extreme dry and hot summer in 2020 of Southern China? (2) What role did human activities have in the occurrence of this extreme summer? (3) What is the relationship between the precipitation deficit and the extreme hot temperatures? (4) What is the likelihood of extreme summer like 2020 in the future?

The rest of the paper is organized as follows. Data and methods used in this study are introduced in section 2. In section 3, we present the results of the observed characteristics of the extremely dry and hot

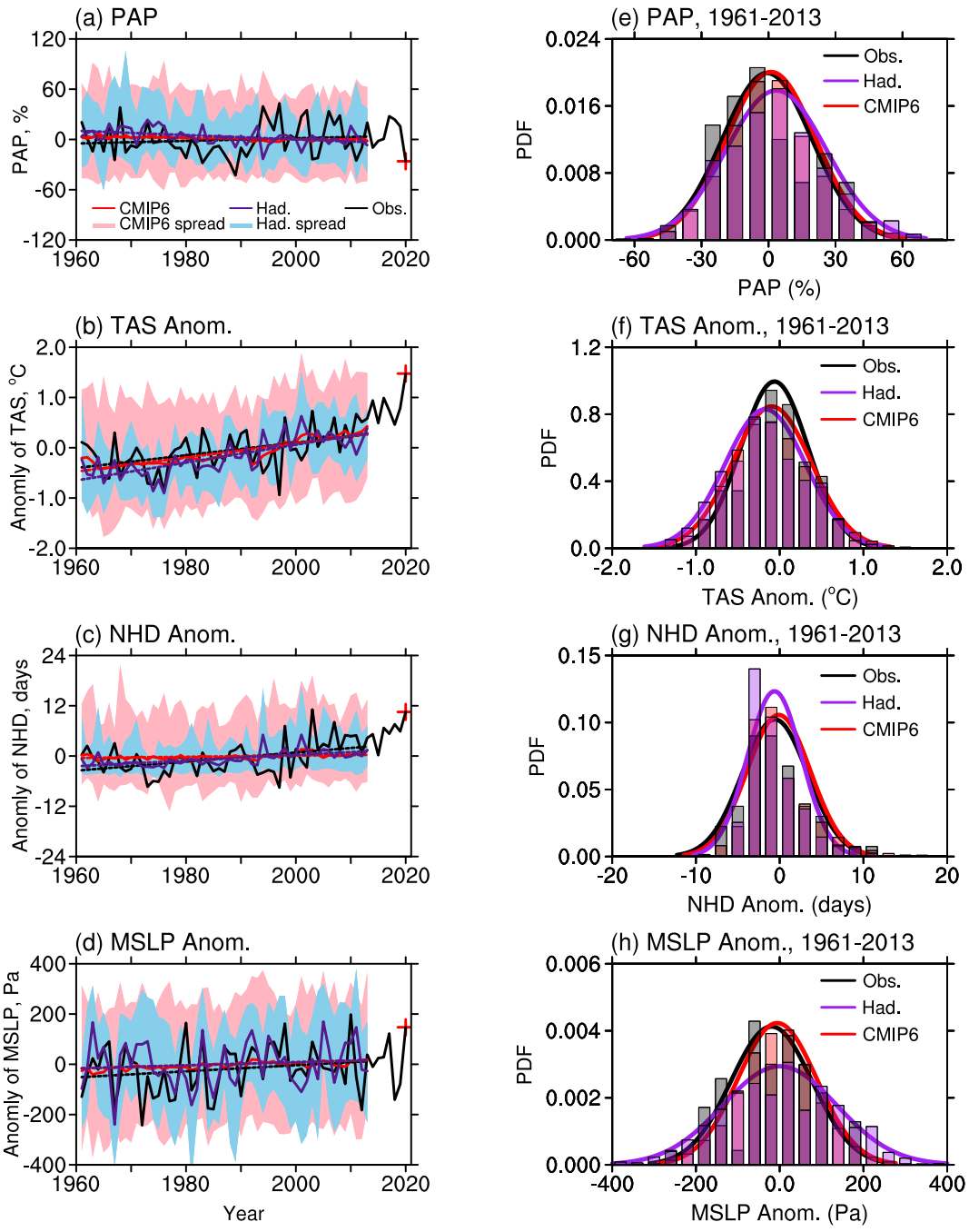

Fig. 3. Timeseries and linear trends of observed (black; 1961–2020) and simulated (1961–2013) ensemble mean Historical and Hist simulations from HadGEM3-GA6 (purple) and CMIP6 (red) June–August (a) PAP, (b) TAS, (c) NHD, and (d) MSLP anomalies, regionally averaged in Southern China [blue box in Fig. 1a–c], with model spread shown as light blue (HadGEM3-GA6) and light pink (CMIP6) shadings, where red crosses denote 2020. Histograms and PDFs of (e) PAP, (f) TAS, (g) NHD, and (h) MSLP anomalies in observations (black), Historical and Hist simulations from HadGEM3-GA6 (purple) and CMIP6 (red) for June–August from 1961 to 2013, regionally averaged in Southern China [blue box in Fig. 1a–c]. (For interpretation of the references to colour in this figure legend, the reader is referred to the Web version of this article.)

summer in 2020 occurring in Southern China and the model performance, and the impact of human activities on this extreme summer. The occurrence probability for extreme summer like 2020 in the future is also investigated. Conclusion and discussions are provided in section 4.

2. Data and methods

2.1. Data

Observation: Gridded observational datasets (0.5° × 0.5°) over China for the period 1961–2020 of daily precipitation, daily mean and daily maximum surface air temperature (TAS, Tmax) are provided by National Meteorological Information Center of China Meteorological Administration (NMIC-CMA). Based on the latest compilation of basic meteorological data from 2 472 national ground meteorological stations (Fig. S1) in China (excluding Xisha and Coral Island stations), using the TPS Thin Plate Spline method combined with three-dimensional geospatial information (longitude, latitude, altitude) for spatial interpolation, the daily ground surface temperature and precipitation gridded point datasets at a horizontal resolution of 0.5° × 0.5° over China are

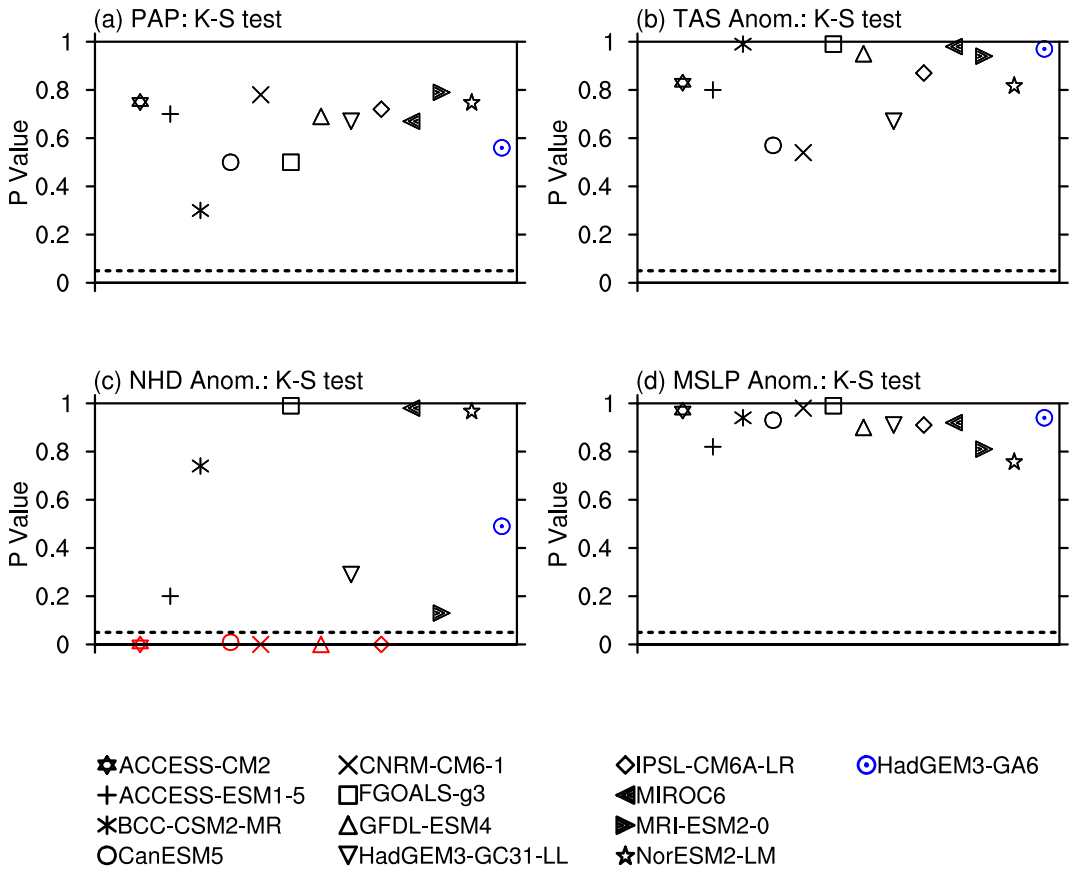

Fig. 4. P-values of K–S test for simulated (a) PAP, (b) TAS, (c) NHD, and (d) MSLP anomalies from HadGEM3-GA6 (blue) and CMIP6 (black). The dotted lines denote the significance level (p-value = 0.05) where the red symbols denote the model failed to pass the K–S test. (For interpretation of the references to colour in this figure legend, the reader is referred to the Web version of this article.)

Table 2
As Table 1, but for the CMIP6 models passed the K–S test (daily maximum temperature).

No.	Model name	Modeling center (or group)	Historical	Hist-nat	SSP2-45	SSP5-85	Spatial resolution (# of Lon × # of Lat)
1	ACCESS-CM2	Commonwealth Scientific and Industrial Research Organisation, Australia	5	–	–	–	192 × 144
2	ACCESS-ESM1-5	Commonwealth Scientific and Industrial Research Organisation, Australia	40	3	40	40	192 × 145
3	BCC-CSM2-MR	Beijing Climate Center, China Meteorological Administration, China	1	3	1	1	320 × 160
4	CanESM5	Canadian Centre for Climate Modelling and Analysis, Environment and Climate Change Canada, Canada	25	–	–	–	128 × 64
5	CNRM-CM6-1	Centre National de RecherchesMétéorologiques, France	1	–	–	–	265 × 128
6	FGOALS-g3	LASG, Institute of Atmospheric Physics, Chinese Academy of Sciences, China	3	3	3	3	180 × 80
7	GFDL-ESM4	National Oceanic and Atmospheric Administration, Geophysical Fluid Dynamics Laboratory, United States	1	–	–	–	288 × 180
8	HadGEM2-GC31-LL	Met Office Hadley Centre, United Kingdom	4	10	4	4	180 × 120
9	IPSL-CM6A-LR	Institution Pierre Simon Laplace, France	11	–	–	–	144 × 143
10	MIROC6	Japan Agency for Marine-Earth Science and Technology, Japan	20	50	20	20	256 × 128
11	MRI-ESM2-0	Meteorological Research Institute, Japan	1	5	1	1	320 × 160
12	NorESM2-LM	NorESM Climate modeling Consortium consisting of Center for International Climate and Environmental Research, Norway	3	3	3	1	144 × 96

established since January 1961. Taking the 2010 data as an example (Fig. S2), the number of stations in the unit grid shows that the coverage rate of stations in the 0.5° × 0.5° grid is 38% in the whole country, while it is as high as 77% in the eastern region (south of 40°N and east of 100°E). These datasets were quality-controlled and homogenized by the NMIC-CMA for the period 1961–2020 (Zhao et al., 2014), which are free and publicly available at http://data.cma.cn/en.

Reanalysis: We used the European Centre for Medium-Range Weather Forecasts Reanalysis 5 (ERA5) data (0.25° × 0.25°) for the period 1981–2020 (Hersbach et al., 2020), including sea level pressure and horizontal wind at 850 hPa.

Model simulations: We used ensembles of HadGEM3-GA6 at N216 resolution, run in atmosphere-only mode with prescribed historical sea surface temperature (SST) and sea ice concentration (SIC) from HadISST, version 1 (Rayner et al., 2003), to investigate how anthropogenic forcings have influenced the probability of the extremely dry and hot summer 2020 in Southern China. The horizontal resolution is 0.56° (latitude) × 0.83° (longitude), approximately equivalent to ~62 km at

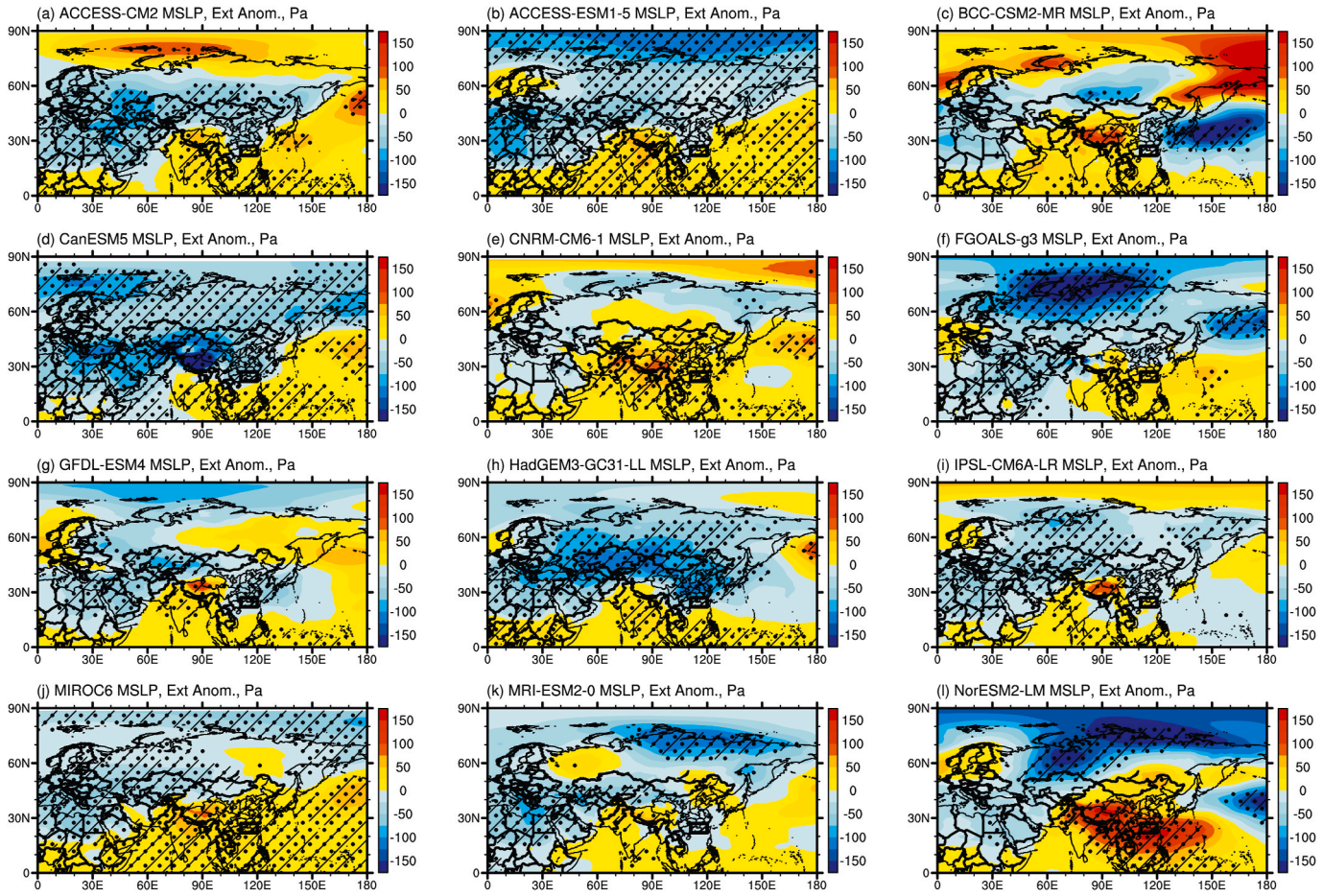

Fig. 5. Spatial patterns of the anomaly in June–August mean sea level pressure (MSLP; shading; Pa) for ensemble mean CMIP6 Historical simulations during 2020 relative to 1981–2010 climatology. The black dots and slash lines denotes 90% and 95% significance level, respectively.

the latitude range and ~95 km longitude range covered by China in this study (Christidis et al., 2013; Ciavarella et al., 2018). Three ensembles were used:

- A 15-member Historical ensemble of outputs from HadGEM3-GA6 for period 1961–2013 (available) was used for model evaluation, in which the model is forced by observed SST and SIC from HadISST, and a comprehensive package of historical anthropogenic and natural forcings (Historical).
- A 525-member ensemble of outputs from HadGEM3-GA6 (factual world), driven as for "Historical" but for 2020 only (HistoricalExt).
- A 525-member ensemble of outputs from HadGEM3-GA6 for 2020 only (counterfactual world), driven with natural forcing, with the anthropogenic influences on SST and SIC removed (HistoricalNatExt).

The HistoricalNatExt (NAT) experiments are provided with SST and SIC fields equal to those provided for Historical (ALL) but from which an estimate of the changes due to anthropogenic influences, ΔSST and ΔSIC, have been removed (Christidis et al., 2013). ΔSST is calculated as the difference between estimates using coupled model simulations of the ALL and NAT scenarios. The HadGEM3-GA6 attribution system currently uses CMIP5 (Taylor et al., 2012) multi-model mean fields for this purpose. ΔSIC is produced through an empirical relationship between historically observed polar SST and SIC. The precise implementation of this method that we have used is described in detail elsewhere (Stone and Pall, 2021).

Model outputs from the Coupled Model Intercomparison Project Phase 6 (CMIP6) archive are used to corroborate the consistency of HadGEM3-GA6 model with observation in this study (Table 1), which are available at https://esgf-node.llnl.gov/search/cmip6/. For attribution analysis, we used the outputs of historical all forcing (Hist) and natural forcing (Hist-nat) experiments from the Detection and Attribution Model Intercomparison Project (DAMIP) in the CMIP6 archive (Gillett et al., 2016; Qian and Zhang 2019), as well as Scenario Model Intercomparison Project (ScenarioMIP) simulations under the Shared Socioeconomic Pathways SSP2-4.5 for 2015–2020. The Hist simulations for 1961–2013 (available) were used for model evaluation. The ScenarioMIP SSP2-4.5 simulation for 2015–2020 was used to estimate event probabilities for 2020. The Hist-nat simulations for 2015–2020 are used to estimate natural probabilities for 2020. To estimate the risk of 2020-like extreme hot and dry summers in the future, we used the outputs of SSP2-4.5 and SSP5-8.5 for 2081–2 100. Detailed information of the CMIP6 experimental design is in Eyring et al. (2016).

2.2. Methods

Three indices were used to define the extreme summer in this study: percentage of anomalous precipitation (PAP), surface air temperature (TAS), and the number of hot days (NHD, Tmax ≥35 °C, defined by CMA). These indices were computed for June–August (JJA) averages over land points in Southern China (22°–27°N, 111°–120°E) and then converted to anomalies against the 1981–2010 climatology. The Chinese observational network is reliable from 1961 (Zhao et al., 2014) and so we rank extreme summers in the 1961–2020 period. NHD is computed at each grid point and then averaged over Southern China. Apart from expressing all results as anomalies no further bias correction was done.

PAP was computed as follows:

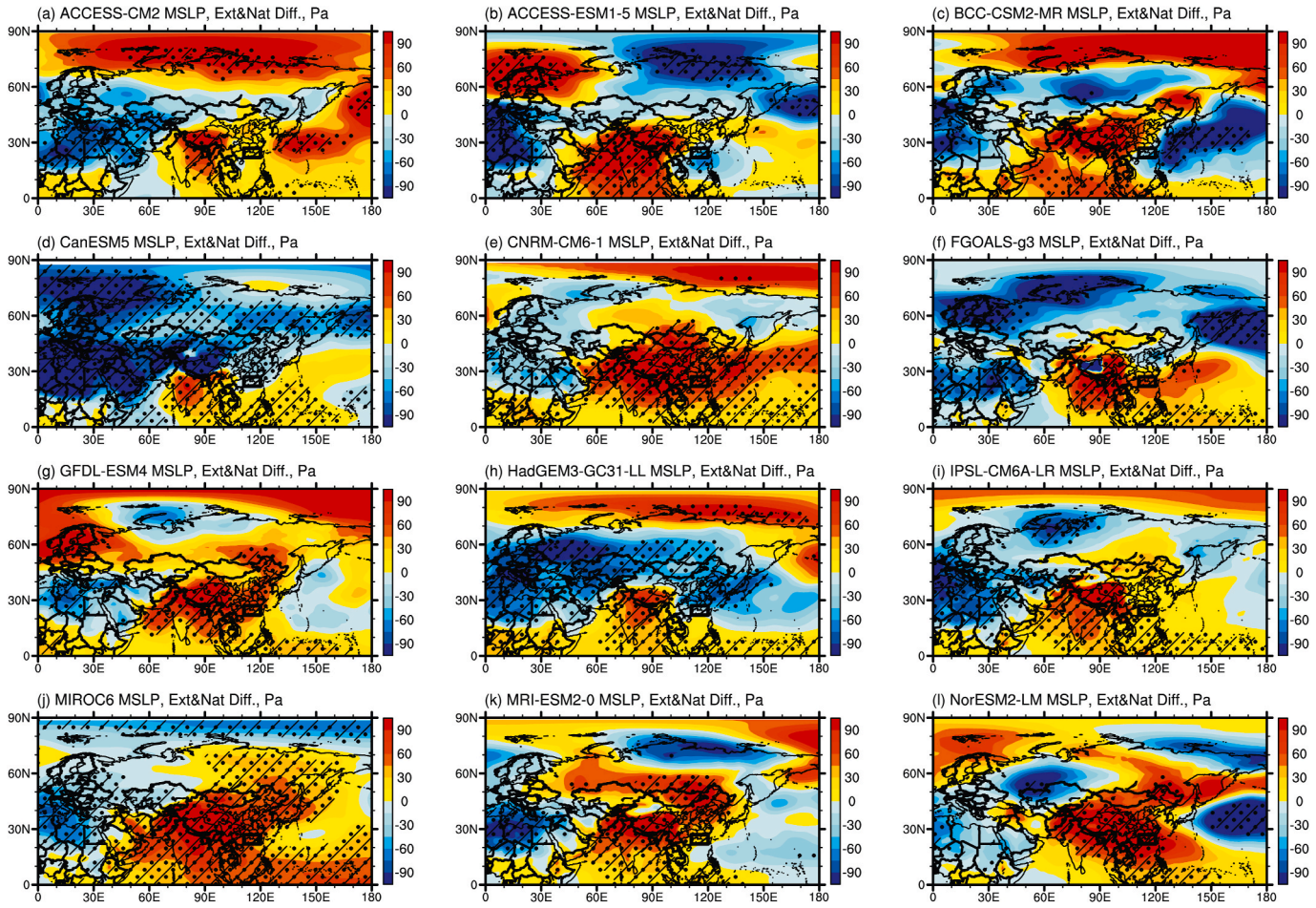

Fig. 6. Spatial patterns of the anomaly in June–August mean sea level pressure (MSLP; shading; Pa) for the difference between ensemble mean CMIP6 Historical and Hist-nat simulations for the year 2020. The black dots and slash lines denotes 90% and 95% significance level, respectively.

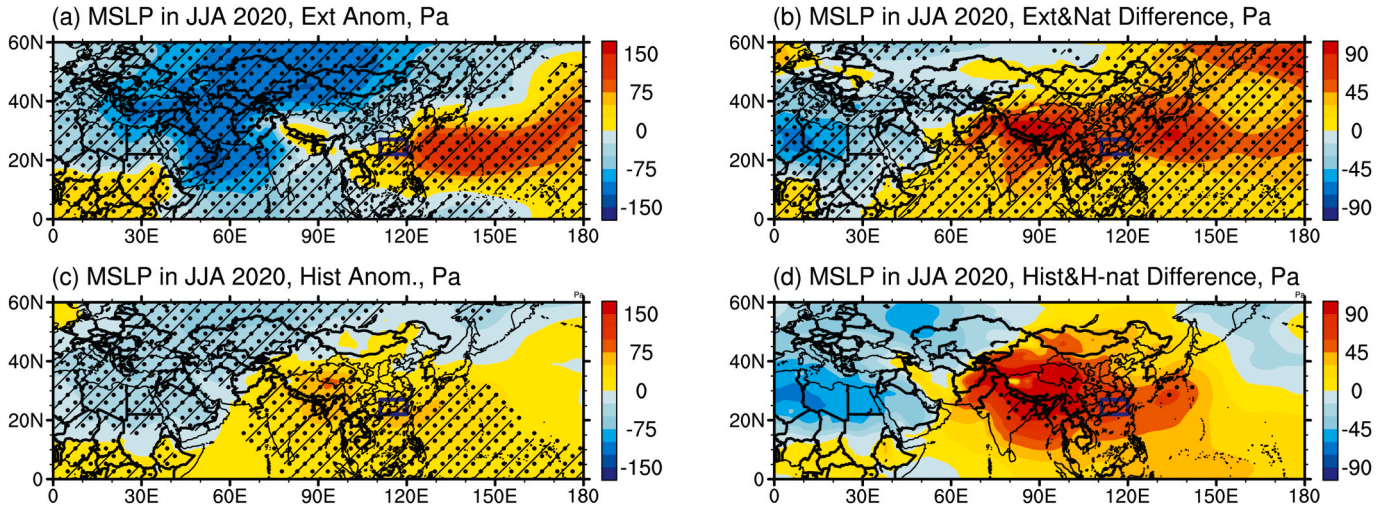

Fig. 7. Spatial patterns of (a) the anomaly in June–August mean sea level pressure (MSLP; shading; Pa) for 525-member ensemble mean HistoricalExt simulations during 2020 relative to 1981–2010 climatology, and (b) the difference between 525-member ensemble mean HistoricalExt and HistoricalNatExt simulations for the year 2020. The black dots and slash lines denotes 90% and 95% significance level, respectively. (c) and (d) are for the multi-member ensemble mean simulations from CMIP6.

$$PAP = \frac{P(x) - \overline{P(1981–2010)}}{P(1981–2010)} \times 100\%$$

Where P is the summer precipitation of a year, x denotes a year during the 1961–2020 period, $\overline{P(1981–2010)}$ is the reference climatology. Here, anomalous precipitation means the deviation of summer mean precipitation of a year from the climatology, as $P(x) - \overline{P(1981–2010)}$.

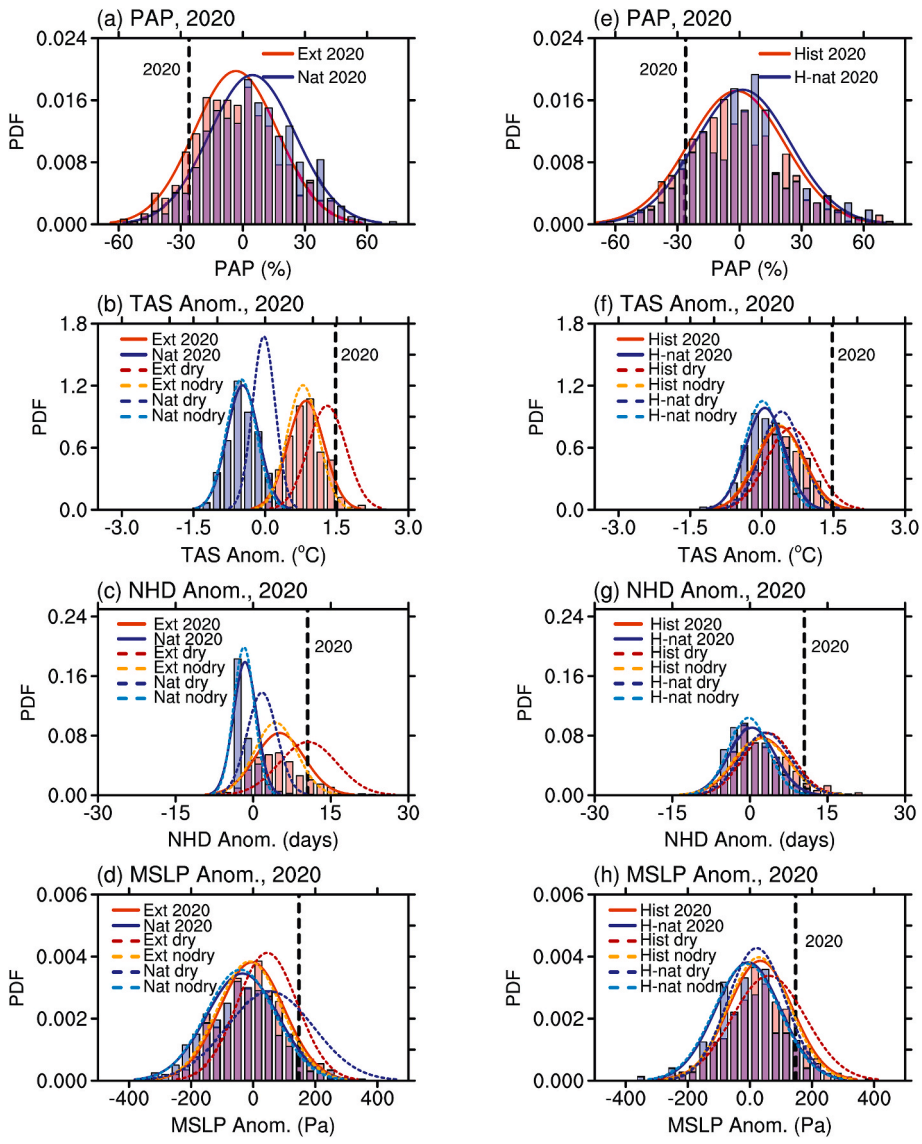

Fig. 8. Histograms and PDFs of (a) PAP, (b) TAS, (c) NHD, and (d) MSLP anomalies in observations (black) and Historical simulations for summer 2020 with 525-member ensemble HistoricalExt (red; all-forcing) and HistoricalNatExt (blue; natural-forcing) simulations from HadGEM3-GA6 for June–August from 1961 to 2013, regionally averaged in Southern China [blue box in Fig. 1a–c]. The orange and light blue dashed lines denote the distributions of TAS and NHD anomalies when PAP $\geq -26.16\%$ (defined as no-dry), the brown and dark blue dashed lines denote the distributions when PAP $< -26.16\%$ (defined as dry). The black dashed lines denote the thresholds for summer 2020. (e), (f), (g), and (h) are for the simulations from CMIP6. (For interpretation of the references to colour in this figure legend, the reader is referred to the Web version of this article.)

The TAS anomaly was computed as follows:

$$\text{TAS anomaly} = \text{T(x)} - \overline{\text{T(1981–2010)}}$$

Where T is the summer mean temperature of a year, x denotes a year during the 1961–2020 period, $\overline{\text{T(1981–2010)}}$ is the reference climatology.

The NHD is defined as the count of days when the daily maximum temperature is greater or equal to 35 °C ($T_{max} \geq 35$ °C) in summer.

In addition, to facilitate the extreme summer analysis, we also computed the mean sea level pressure (MSLP) anomaly using the same calculation as TAS anomaly.

To estimate probabilities, a Normal distribution was fit to the four indices from two 525-member ensembles of 2020 for HadGEM3-GA6 and several hundred samples of 2015–2020 for CMIP6. A two-sided Kolmogorov-Smirnoff (K–S) test was used to test if the distributions of observations and Historical/Hist simulations from 1961 to 2013 are from the same population and to test if the distributions used to fit the indices are appropriate. For the CMIP6 multi-model ensemble, we tested each model separately. If the indices failed test, we remove the model from the simulation of that indices. Linear trends in the simulations and observations were tested for significance using a *t*-test at the 95% level.

To estimate the anthropogenic influences on the probability of this kind of summer, probability ratio (PR, Fischer and Knutti, 2015) was calculated by $P_{HistoricalExt}/P_{HistoricalNatExt}$ in HadGEM3-GA6 and $P_{Hist}/P_{Hist\text{-}nat}$ in CMIP6.

$$PR_{HadGEM3\text{-}GA6} = \frac{P_{HistoricalExt}}{P_{HistoricalNatExt}}, PR_{CMIP6} = \frac{P_{Hist}}{P_{Hist\text{-}nat}}$$

Where $P_{HistoricalExt}$ and P_{Hist} are the probabilities of the summer in the factual world, and $P_{HistoricalNatExt}$ and $P_{Hist\text{-}nat}$ are in the counterfactual world, respectively (Fischer and Knutti, 2015; Easterling et al., 2016). We calculate the probability of PAP, TAS, NHD and MSLP anomalies larger than the observed 2020 values from the fitted distributions. PR uncertainty was estimated via bootstrapping 1 000 times, by resampling

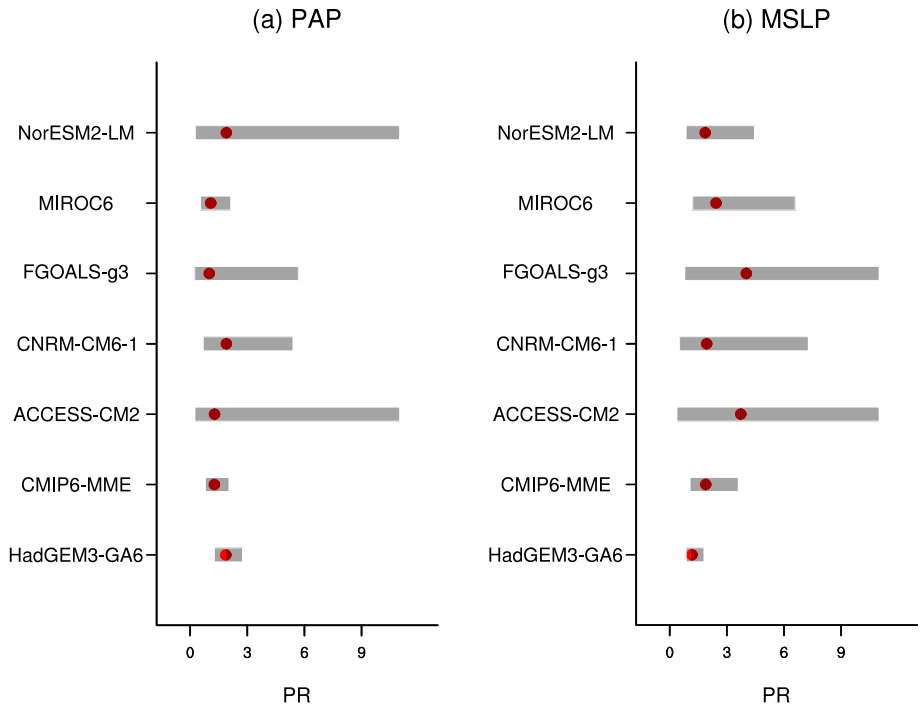

Fig. 9. Probability ratio (PR) of (a) PAP and (b) MSLP anomaly from HadGEM3-GA6 and CMIP6 simulations. The horizontal grey bars denote the 2.5%–97.5% uncertainty range for PR. The red solid dots denote the values of PR. (For interpretation of the references to colour in this figure legend, the reader is referred to the Web version of this article.)

Table 3
Probability of TAS, NHD and MSLP anomalies under different precipitation thresholds conditions from HadGEM3-GA6 and CMIP6.

	HadGEM3-GA6		CMIP6	
PR	PAP > -26%	PAP < -26%	PAP > -26%	PAP < -26%
TAS	0.02	0.33	0.01	0.04
NHD	0.06	0.55	0.06	0.07
MSLP	0.06	0.15	0.12	0.23

all ensemble members with replacement, which is a Gaussian process, rather than a physically based one. We then computed 1 000 PR bootstrap samples and used them to estimate PR uncertainty with the 95% confidence interval (95% CI, 2.5%–97.5%) based on the "likelihood ratio method" (Paciorek et al., 2018).

3. Results

3.1. Observed extreme summer and model performance

In parts of Southeastern China in the summer of 2020, PAP is up to 60% lower than normal years (Fig. 1a), seasonal-mean TAS anomaly over most areas is more than 1 °C and reaches 1.8 °C in northern parts (Fig. 1b), and the NHD anomaly exceeds 18 days (Fig. 1c). As for the regional mean, PAP is about 26% below the climatology and is the 4th driest in 1961–2020 record (Fig. 1d), TAS anomaly is about 1.5 °C and breaks the record (Fig. 1e), and the NHD anomaly is about 11 days and is the 2nd highest (Fig. 1f). Return periods (RPs) for the observed 2020 dry and hot summer are about once in 16, 80, and 50 years for PAP, TAS, and NHD anomalies, respectively. To define extreme summer like, or larger, than summer 2020 we use thresholds of −26%, 1.5 °C, and 11 days for PAP, TAS and NHD anomalies, respectively.

The Western Pacific Subtropical High (WPSH) is one of most important factors affecting the summer climate in Southern China, the large-scale descent anomaly caused by westward shift and strengthening of the WPSH is the direct cause of high temperatures (Fig. S3a) in 2020 over Southern China. Considering the WPSH is closely associated with global warming, we used mean sea level pressure (MSLP) instead of the WPSH in this study, which agrees well with WPSH and shows a high correlation in Southern China areas (Fig. S3b). The correlation coefficient between MSLP and TAS in Southern China is statistically significant at the 90% confidence level (Fig. S3c). That means the MSLP is one of the important factors influencing TAS. The highest MSLP anomaly value of 200 Pa appears in parts of Southeastern China in the summer of 2020 (Fig. 2a), and the regional mean MSLP anomaly is about 150 Pa which is the 4th highest in 1961–2020 (Fig. 2b). Return period (RP) for the observed 2020 dry and hot summer is about once in 15 years for MSLP anomaly (Fig. 2c). We also used thresholds of 150 Pa for the anomaly of MSLP to define extreme summer like, or larger, than summer 2020.

The positive anomalies of MSLP in 2020 covering Southeastern China, the central-northern South China Sea (SCS), and the western Pacific, which is accompanied by easterly wind anomalies in the Philippine Sea, the central-southern SCS, the Indochina peninsula, and the Bay of Bengal regions in the lower troposphere (Fig. 2a). These circulation anomalies were connected with the Indian Ocean Dipole that occurred in the autumn of in the previous year, which triggered easterly wind anomalies and induced anticyclonic circulation anomalies in the western Pacific (Wang et al., 2021; Zhou et al., 2021). The persistent anomalous anticyclonic circulation over Southern China facilitates the regional increase of surface solar radiation and adiabatic heating (Chen et al., 2016, 2018), contributing to the dry and hot summer of 2020. In addition, the persistency and enhancement of WPSH could also boost the lower level anticyclone over the west Pacific (Yao and Wang 2021).

For 1961–2013 both observations and HadGEM3-GA6 Historical simulations have positive trends for TAS (0.12 vs 0.17 °C/decade), NHD (1.08 vs 0.68 day/decade) and MSLP (12.1 vs 6.7 Pa/decade). All are statistically significant at the 95% level (Fig. 3b–d; black and purple dashed lines), showing a better model performance. As for PAP, the envelope of simulated PAP across model simulations encompasses the observed change, although observations show a weak positive trend of

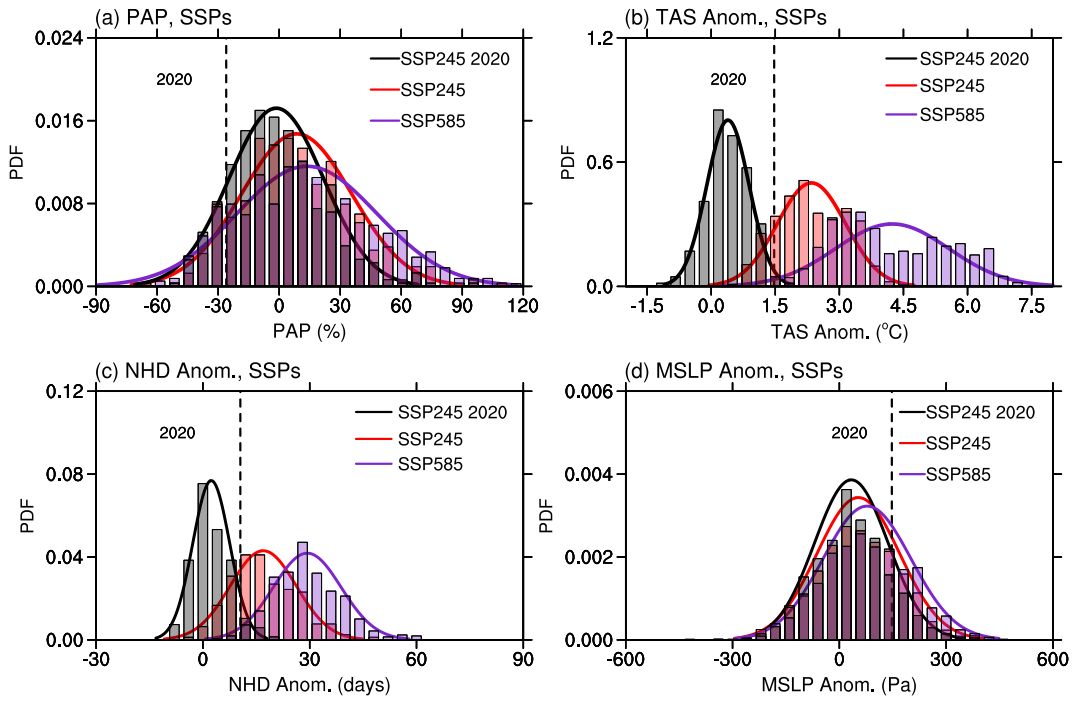

Fig. 10. Histograms and PDFs of (a) PAP, (b) TAS, (c) NHD, and (d) MSLP anomalies in SSP245 scenario simulations for the 2020 summer (black), and in SSP245 (red) and SSP585 (purple) scenarios simulations for June–August during 2081–2100, regionally averaged in Southern China [blue box in Fig. 1a–c]. The black dashed lines denote the thresholds for summer 2020. (For interpretation of the references to colour in this figure legend, the reader is referred to the Web version of this article.)

1.6%/decade, while HadGEM3-GA6 Historical simulations exhibit the little drying trend of −2.6%/decade (Fig. 3a). Similar results were found for the CMIP6 Hist simulations with multi-member ensemble mean trends of −0.8%/decade, 0.14 °C/decade, 0.22 days/decade and 6.2 Pa/decade for PAP, TAS, NHD and MSLP anomalies (Fig. 3a–d; red dashed lines), respectively.

Probability distribution functions (PDFs) of observed and simulated PAP, TAS, NHD, and MSLP anomalies for June–August 1961–2013 are statistically indistinguishable based on K–S tests at a p-value of 0.05, $p_{(PAP)} = 0.56$, $p_{(TAS)} = 0.97$, $p_{(NHD)} = 0.49$, and $p_{(MSLP)} = 0.94$ for Historical simulations from HadGEM3-GA6 (Fig. 3e–h; purple solid curves; Fig. 4). PDFs of observed and CMIP6 Hist ensemble PAP, TAS, NHD and MSLP anomalies for the same period are also statistically indistinguishable based on K–S tests at a p-value of 0.05, $p_{(PAP)} = 0.63$, $p_{(TAS)} = 0.87$, $p_{(NHD)} = 0.46$ and $p_{(MSLP)} = 0.85$ (Fig. 3e–h; red solid curves; Fig. 4; Table 2). It should be noted that the PDFs of NHD anomalies in CMIP6 (Fig. 3g) exclude the poor-performing models, which are ACCESS-CM2, CanESM5, CNRM-CM6-1, GFDL-ESM4, and IPSL-CM6A-LR due to their failure to reproduce the observed cumulative distribution function. (Fig. 4c). Spatial patterns of the anomaly in June–August MSLP during 2020 relative to 1981–2010 climatology for CMIP6 Historical simulation have high model dependence (Fig. 5). Five models (ACCESS-CM2, CNRM-CM6-1, FGOALS-g3, MIROC6 and NorESM2-LM) can reproduce the anomalous MSLP of 2020 summer in Southern China and Northwest Pacific regions. Therefore, simulations from ACCESS-CM2, CNRM-CM6-1, FGOALS-g3, MIROC6 and NorESM2-LM were used to attribution analysis.

3.2. Impact of human activities

Firstly, simulated summer MSLP from ACCESS-CM2, CNRM-CM6-1, FGOALS-g3, MIROC6 and NorESM2-LM were abnormally high across East Asia and the Northwest Pacific in Historical than Hist-nat simulations for the year 2020, with values of nearly 100 hPa in Southern China (Fig. 6). HadGEM3-GA6 HistoricalExt simulations captures the anomalous MSLP in the 2020 summer strength though with a magnitude weaker than observation (Fig. 7a). Summer MSLP was abnormally high across East Asia and the Northwest Pacific in HistoricalExt than HistoricalNatExt, with values of nearly 100 hPa in Southern China (Fig. 7b), means that human activities can influence the positive anomalies of MSLP, thus favor the occurrence of dry and hot summer. Results from multi-member ensemble mean in CMIP6 (Fig. 7c and d) is consistent with HadGEM3-GA6 simulations.

There is a leftward shift of the PAP probability curve in HistoricalExt from 525-member ensembles in 2020 compared to in HistoricalNatExt, indicating that anthropogenic influences have increased the probability of a drier 2020-like summer (Fig. 8a). For PAP < −26%, the probability in HistoricalNatExt ($P_{HistoricalNatExt}$) is 0.07 (RP about 16 years) while $P_{HistoricalExt}$ is 0.13 (RP about 8 years), giving a rough doubling of the probability of such precipitation deficit (95% CI: 1.27–2.75). Distributions of TAS anomaly in HistoricalExt are considerably warmer than those of HistoricalNatExt. A warming of >1.5 °C, like the 2020 summer with a 20-year RP (probability of 0.05), has a probability less than 10^{-8} in HistoricalNatExt (Fig. 8b). The NHD anomaly distribution in HistoricalExt also shifts rightward relative to HistoricalNatExt (probability of 0.13, RP about 8 years) and the probability in NHD anomalies >11 days in HistoricalNatExt is also less than 10^{-8} (Fig. 8c). The PRs for both TAS and NHD are large than 10^6. A minor change occurs in the MSLP probability, with $P_{HistoricalExt}$ is 0.07 (RP about 14 years) and $P_{HistoricalNatExt}$ is 0.06 (RP 17 years) (Fig. 8d). The probability of MSLP anomalies >150 Pa increased by 17% (95% CI: 0.86–1.80) from $P_{HistoricalNatExt}$ to $P_{HistoricalExt}$, showing that human activities have also increased the probability of 2020-like summer MSLP anomalies, which agree with the enhanced anticyclonic circulation anomaly over Southern China and the western Pacific in Fig. 7b.

For CMIP6 multi-model ensembles results, the probability of PAP < −26% in Hist-nat ($P_{Hist\text{-}nat}$) is 0.11 (RP of about 9 years) while P_{Hist} is 0.14 (RP of about 7 years) with a PR of 1.27 (95% CI:0.80–2.04) (Fig. 8e), showing that human activities have no significant influence to PAP. We calculated PR in PAP for each model, the PR ranges (95% CI:

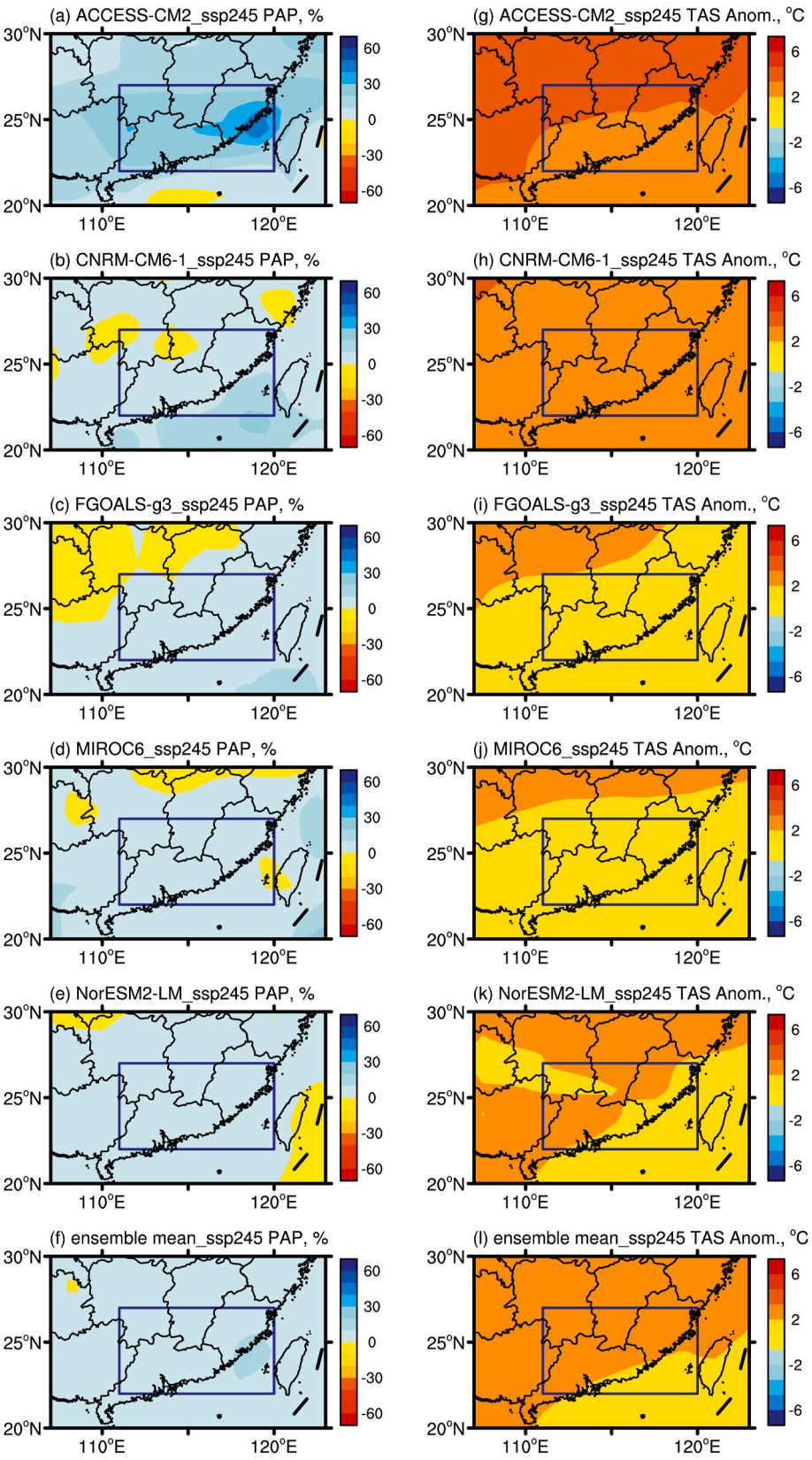

Fig. 11. Spatial patterns of (a–f) PAP (%) and (g–l) TAS (°C) anomalies in SSP245 scenario simulations for June–August during 2081–2100, respectively.

0.24–15) are much larger (Fig. 9a), showing the large uncertainties in PAP attribution. The probability of TAS/NHD anomaly above 1.5 °C/11 days is 0.01/0.06 (RP about 100/17 years) in Hist and is about 1.9 × 10^{-4}/ 0.01 in Hist-nat, leaving to PRs with 52.63 (95% CI: 11.10–602.9) and 6.00 (95% CI: 1.25–20.52) (Fig. 8f and g). The probability of MSLP anomaly over 150 Pa is 0.14 in Hist (RP about 7 years) and 0.07 (RP about 14 years) in Hist-nat (Fig. 8h), human activities lead to a 100% (95% CI: 1.07–3.60) increase in the probability. We also calculated the

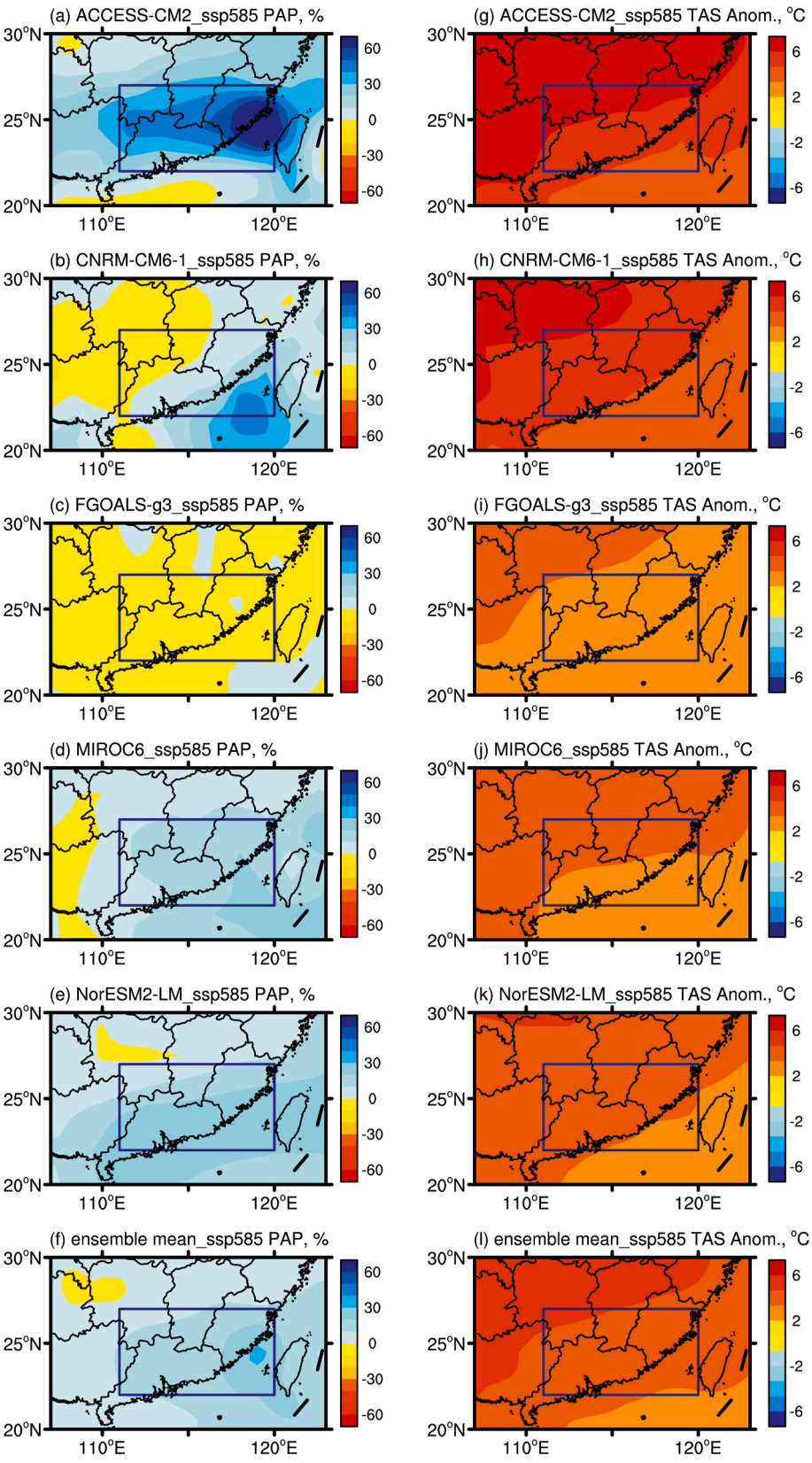

Fig. 12. Same as for Fig. 11, but for SSP585 scenario.

PR of MSLP for each CMIP6 model (Fig. 9b), large uncertainties remain in MSLP by considerable model spread.

To investigate the relevance of precipitation deficit to TAS, NHD and MSLP anomaly, a given PAP value of −26% of 2020-like was used for conditional analysis. Simulations are divided into two groups with the threshold below/above being termed as dry/no-dry. Dry simulations shift TAS, NHD and MSLP anomaly PDFs rightwards in both "factual" and "counterfactual" simulations (Fig. 8b–d and Fig. 8f–h). Here

"factual" simulations (HistoricalExt in HadGEM3-GA6 and Hist in CMIP6) were used to analyze the changes of probability under dry and no-dry with thresholds of 2020 summer, as shown in Table 3. The occurrence probability of dry and hot summer is much higher under a dry background than no-dry. PR calculated by $P_{(dry)}/ P_{(no\_dry)}$ shows that precipitation deficits increase the probability of hot summer intensively in "factual" simulations. The PRs for TAS, NHD and MSLP anomalies are 16.50 (95% CI: 8.00–31.44), 9.20 (95% CI: 5.20–14.01) and 2.50 (95% CI: 1.14–4.26) in HadGEM-GA6, 4.00 (95% CI: 0.61–14.52), 1.31 (95% CI: 0.11–6.68) and 1.94 (95% CI: 0.91–3.59) in CMIP6, respectively.

3.3. Projected risk under the future scenarios

We investigated the changes of occurrence probability for the extreme summer like 2020 in the future using the CMIP6 multi-model ensemble forced with the SSP2-4.5 and SSP5-8.5 scenarios in 2081–2 100 (Fig. 10). Negative changes in PAP probability can be found in SSP2-4.5 and SSP5-8.5 with values of 0.041 and 0.042 in 2081–2100, compared to 0.09 in 2020 (Fig. 10a), indicating a tendency towards less drying in the future. Human influences lead to more frequent hot summers in SSP5-8.5 than in SSP2-4.5, the probability of TAS anomaly exceeding the 1.5 °C threshold is projected to increase to 0.97 in SSP2-4.5 and nearly 1 in SSP5-8.5 during 2081–2 100 period (Fig. 10b), as well as 0.54 and 0.87 for NHD anomaly with a threshold of 11 days above (Fig. 10c). As shown in Fig. 10d, PDFs for MSLP anomaly will be flatter under SSP2-4.5 in 2081–2 100 than in 2020. For a given 150 Pa MSLP anomalies threshold, a flatter probability shape indicates that the extremely anomalous MSLP events will increase in both occurrence and intensity. The PRs (calculated by $P_{(2081–2\ 100)}/ P_{(2020)}$) for PAP, TAS, NHD and MSLP anomaly in SSP2-4.5 are 0.71, 86.00, 12.67 and 1.54, with 95% CI: 0.47–1.00, 42.56–108.64, 7.89–26.67, 1.15–2.05, respectively. In SSP5-8.5, they are 0.86, 98.00, 16.33 and 2.11 with 95% CI: 0.59–1.17, 50.26–122.22, 10.78–32.67, 2.11–2.77. That means the strength and frequency of extreme summer will increase in Southern China during 2081–2 100 and future summer will be characterized by wet and hot summer instead of dry and hot summer (Fig. 10). Spatial patterns of PAP and TAS anomalies in SSP2-4.5 and SSP5-8.5 scenarios simulations for June–August during 2081–2 100 in Southern China also show a wet and hot summer in the future (Figs. 11 and 12).

4. Conclusions and discussion

In summer 2020, Southern China was impacted by exceptionally precipitation deficit and high temperatures, which was characterized by the 4th driest, the highest temperature, and the 2nd highest number of hot days in the record during the 1961–2020 period. The impact of human activities on the 2020 summer anomalous climate in Southern China was investigated by factual and counterfactual runs from 525-member ensemble simulations with the atmosphere-only model HadGEM3-GA6 and multi-model ensemble results with CMIP6.

Anthropogenic forcings have contributed to the increase in the probability of a 2020-like hot summer at a regional scale, but there are uncertainties regarding on the dry summer. The observed 2020 TAS and NHD anomalies cannot be reproduced in HadGEM3-GA6 without human influences, while in CMIP6 probability ratios are more than 50 and 6. Simulated probabilities exceeding the −26% observed PAP threshold have roughly doubled in HadGEM3-GA6 simulations and by about 27% increase in CMIP6 simulations due to anthropogenic influences. Similarly, occurrences of 2020-like MSLP anomalies increased by 17% in HadGEM3-GA6 and 100% in CMIP6. However, the uncertainty analysis for PAP in CMIP6 and MSLP in HadGEM3-GA6, showing a PR of less than 1 with the 95% CI, indicate that there is no robust evidence that human influences have changed the circulation and rainfall over Southern China.

PAP is closely connected to TAS, NHD and MSLP anomalies under anthropogenic influences. For precipitation deficit conditions of the 2020-like summer, the probability of observed 2020 TAS, NHD and MSLP anomalies increase about 17/4, 9/1 and 3/2 times in HadGEM3-GA6/CMIP6 ensembles for the dry cases compared to the no-dry cases. The dry conditions (precipitation deficit) increased the likelihood of exceeding the observed thresholds for both TAS and NHD.

Projections under the SSP2-4.5 and SSP5-8.5 scenarios show that the 2020-like hot summer will likely occur more frequently, while the dry summer occurs less frequently. In addition, the hot and wet extreme summers will increase in intensity and frequency in the future, shown by a flatter and rightward shifted probability density function.

It is still a challenge to attribute compound extreme events such as dry and hot summers in recent years, especially for the attribution of anthropogenic forcing. The relationship between dry and hot summers also needs to be further discussed (Koster et al., 2019; Yu and Zhai, 2020). The results of this study show that human activities have an obvious impact on the occurrence of hot extreme summer. The positive feedback between the dry and hot summer like 2020 in Southern China supports the view of coupling between them in exacerbating the severity of concurrent dry and hot summer. Several studies found the intensity of observed precipitation is always increasing but the duration tends to shorten, which can potentially lead to a decrease in the total rainfall. This phenomenon may be common in the tropics and middle latitude regions, when temperatures exceed a certain threshold limit (Utsumi et al., 2011). However, findings about anthropogenic influences vary in the 2081–2 100 period, this may be explained by the Clausius-Clapeyron (C–C) relationship (Trenberth, 1999). Column-integrated water vapor content increases with approximately 7% per 1 °C of global-mean surface warming, and average and extreme precipitation in most humid region is projected to increase with temperature rise (IPCC et al., 2021). Our results are consistent with these conclusions.

Our conclusions still have limitations. Simulated PAP shows a slightly decreasing trend, opposite to what occurred in observations, which may influence attribution conclusions, although neither observation nor simulation trends are statistically significant. Consistent findings from HadGEM-GA6 and CMIP6 simulations increase the confidence for conclusions that anthropogenic forcing increases the probability of hot summer in Southern China.

CRediT authorship contribution statement

Kaixi Wang: Writing – review & editing, Writing – original draft, Methodology, Investigation, Formal analysis, Data curation, Conceptualization. **Zhiyuan Zheng:** Writing – review & editing, Writing – original draft, Supervision, Methodology, Investigation, Formal analysis, Conceptualization. **Xian Zhu:** Methodology, Investigation, Formal analysis, Data curation, Conceptualization. **Wenjie Dong:** Supervision. **Simon F.B. Tett:** Writing – review & editing, Supervision, Methodology, Formal analysis, Conceptualization. **Buwen Dong:** Writing – review & editing, Validation, Supervision, Methodology, Formal analysis. **Wenxia Zhang:** Supervision. **Fraser C. Lott:** Supervision. **Lulei Bu:** Formal analysis, Conceptualization. **Yumiao Wang:** Methodology, Formal analysis, Conceptualization. **Huixin Li:** Formal analysis, Conceptualization. **Nergui Nanding:** Supervision, Methodology. **Nicolas Freychet:** Supervision. **Dongqian Wang:** Data curation. **Shaobo Qiao:** Supervision, Formal analysis.

Declaration of competing interest

The authors declare that they have no known competing financial interests or personal relationships that could have appeared to influence the work reported in this paper.

Data availability

The surface air temperature dataset for 1961 to 2020 is available at http://www.nmic.

cn/data/detail/dataCode/SURF_CLI_CHN_TEM_DAY_GRID_0.5.html.

The precipitation dataset for 1961 to 2020 is available at http://www.nmic.cn/data/detail/dataCode/SURF_CLI_CHN_PRE_DAY_GRID_0.5.html.

The sea level pressure and horizontal wind for the period from 1981 to 2020 are available at https://cds.climate.copernicus.eu/cdsapp#!/dataset/reanalysis-era5-pressure-levels-monthly-means?tab=form.

The HadGEM3-GA6 datasets are provided by https://doi.org/10.1016/j.wace.2018.03.003 (Ciavarella et al., 2018).

The model output data from the CMIP6 archive used in this study is available at https://esgf-node.llnl.gov/search/cmip6/.

Acknowledgments

This work was supported by funding to ZZ, XZ and WD from the Guangdong Major Project of Basic and Applied Basic Research (2020B0301030004). ZZ acknowledges the National Natural Science Foundation of China (42005114). ZZ, XZ and WD acknowledge the Second Tibetan Plateau Scientific Expedition and Research Program (2019QZKK0103). KW, ZZ, WD, XZ, SQ acknowledge the Innovation Group Project of Southern Marine Science and Engineering Guangdong Laboratory (Zhuhai) (311022006). HL acknowledges the National Natural Science Foundation of China (42005015). SFBT, BD, FL, and NF acknowledge the UK-China Research & Innovation Partnership Fund through the Met Office Climate Science for Service Partnership (CSSP) China as part of the Newton Fund. NN acknowledges the National Natural Science Foundation of China (41905101, 41975113, and 41861144014). We are very grateful to the editor and the two anonymous referees for their careful reviews and valuable comments, which led to substantial improvement of this work.

Appendix A. Supplementary data

Supplementary data to this article can be found online at https://doi.org/10.1016/j.wace.2024.100706.

References

Bador, M., Terray, L., Boé, J., Somot, S., Alias, A., Gibelin, A.-L., Dubuisson, B., 2017. Future summer mega-heatwave and record-breaking temperatures in a warmer France climate. Environ. Res. Lett. 12 (7), 074025.

Burke, C., Stott, P., 2017. Impact of anthropogenic climate change on the east Asian summer monsoon. J. Clim. 30 (14), 5205–5220.

Chen, R.D., Wen, Z.P., Lu, R.Y., 2016. Evolution of the circulation anomalies and the Quasi-Biweekly oscillations associated with extreme heat events in southern China. J. Clim. 29 (19), 6909–6921.

Chen, R.D., Wen, Z.P., Lu, R.Y., 2018. Large-scale circulation anomalies and intraseasonal oscillations associated with long-lived extreme heat events in south China. J. Clim. 31 (1), 213–232.

Chen, Y., Chen, W., Su, Q., Luo, F.F., Sparrow, S., Tian, F.X., Dong, B.W., Tett, S.F.B., Lott, F.C., Wallom, D., 2019. Anthropogenic warming has substantially increased the likelihood of july 2017–like heat waves over central eastern China. Bull. Am. Meteorol. Soc. 100 (1), S91–S95.

Christidis, N., Stott, P.A., Scaife, A.A., Arribas, A., Jones, G.S., Copsey, D., Knight, J.R., Tennant, W.J., 2013. A new HadGEM3-A-based system for attribution of weather- and climate-related extreme events. J. Clim. 26 (9), 2756–2783.

Ciavarella, A., Christidis, N., Andrews, M., Groenendijk, M., Rostron, J., Elkington, M., Burke, C., Lott, F.C., Stott, P.A., 2018. Upgrade of the HadGEM3-A based attribution system to high resolution and a new validation framework for probabilistic event attribution. Weather Clim. Extrem. 20, 9–32.

Devanand, A., Evans, J.P., Abramowitz, G., Hobeichi, S., Pitman, A.J., 2023. What is the probability that a drought will break in Australia? Weather. Clim. Extrem. 41, 100598.

Dong, S.Y., Sun, Y., Li, C., 2020. Detection of human influence on precipitation extremes in Asia. J. Clim. 33 (12), 5293–5304.

Easterling, D.R., Kunkel, K.E., Wehner, M.F., Sun, L.Q., 2016. Detection and attribution of climate extremes in the observed record. Weather Clim. Extrem. 11, 17–27.

Eyring, V., Bony, S., Meehl, G.A., Senior, C.A., Stevens, B., Stouffer, R.J., Taylor, K.E., 2016. Overview of the coupled model intercomparison project Phase 6 (CMIP6) experimental design and organization. Geosci. Model Dev. (GMD) 9 (5), 1937–1958.

Fischer, E.M., Knutti, R., 2015. Anthropogenic contribution to global occurrence of heavy-precipitation and high-temperature extremes. Nat. Clim. Change 5 (6), 560–564.

Gillett, N.P., Shiogama, H., Funke, B., Hegerl, G., Knutti, R., Matthes, K., Santer, B.D., Stone, D., Tebaldi, C., 2016. The detection and attribution model intercomparison project (DAMIP v1.0) contribution to CMIP6. Geosci. Model Dev. (GMD) 9 (10), 3685–3697.

González-Reyes, Á., Jacques-Coper, M., Bravo, C., Rojas, M., Garreaud, R., 2023. Evolution of heatwaves in Chile since 1980. Weather Clim. Extrem. 41, 100588.

Hersbach, H., Bell, B., Berrisford, P., Hirahara, S., Horányi, A., Muñoz-Sabater, J., Nicolas, J., Peubey, C., Radu, R., Schepers, D., Simmons, A., Soci, C., Abdalla, S., Abellan, X., Balsamo, G., Bechtold, P., Biavati, G., Bidlot, J., Bonavita, M., Chiara, G., Dahlgren, P., Dee, D., Diamantakis, M., Dragani, R., Flemming, J., Forbes, R., Fuentes, M., Geer, A., Haimberger, L., Healy, S., Hogan, R.J., Hólm, E., Janisková, M., Keeley, S., Laloyaux, P., Lopez, P., Lupu, C., Radnoti, G., Rosnay, P., Rozum, I., Vamborg, F., Villaume, S., Thépaut, J.N., 2020. The ERA5 global reanalysis. Q. J. R. Meteorol. Soc. 146 (730), 1999–2049.

Holgate, C.M., Pepler, A.S., Rudeva, I., Abram, N.J., 2023. Anthropogenic warming reduces the likelihood of drought-breaking extreme rainfall events in southeast Australia. Weather Clim. Extrem. 42, 100607.

IPCC, 2021. Climate change 2021: the physical science basis. In: Masson-Delmotte, V., Zhai, P., Pirani, A., Connors, S.L., Péan, C., Berger, S., Caud, N., Chen, Y., Goldfarb, L., Gomis, M.I., Huang, M., Leitzell, K., Lonnoy, E., Matthews, J.B.R., Maycock, T.K., Waterfield, T., Yelekçi, O., Yu, R., Zhou, B. (Eds.), Contribution of Working Group I to the Sixth Assessment Report of the Intergovernmental Panel on Climate Change. Cambridge University Press, Cambridge, United Kingdom and New York, NY, USA, p. 2391.

Koster, R.D., Schubert, S.D., Wang, H., Mahanama, S.P., DeAngelis, A.M., 2019. Flash drought as captured by reanalysis data: disentangling the contributions of precipitation deficit and excess evapotranspiration. J. Hydrometeorol. 20 (6), 1241–1258.

Kumar, M.D., Viswanathan, P.K., Bassi, N., 2015. Water scarcity and pollution in south and Southeast Asia: problems and challenges. In: Harris, P.G., Lang, G. (Eds.), Routledge Handbook of Environment and Society in Asia. Taylor and Francis Group, London, pp. 197–215. Routledge.

Li, R.K., Li, D.L., Nanding, N., Wang, X., Fan, X.W., Chen, Y., Tian, F.X., Tett, S.F.B., Dong, B.W., Lott, F.C., 2021. Anthropogenic influences on heavy precipitation during the 2019 extremely wet rainy season in southern China. Bull. Am. Meteorol. Soc. 102 (1), S103–S109.

Li, W.G., Hou, M.T., Chen, H.L., Chen, X.M., 2012. Study on drought trend in south China based on standardized precipitation evapotranspiration index. J. Nat. Disasters 21 (4), 84–90 in Chinese.

Lo, S.-H., Chen, C.-T., Hsu, H.-H., Shih, M.-F., Liang, H.-C., 2023. The unprecedented spatial extent and intensity of the 2021 summer extreme heatwave event over the Western North American regions. Weather Clim. Extrem. 41, 100576.

Lo, S.-H., Chen, C.-T., Russo, S., Huang, W.-R., Shih, M.-F., 2021. Tracking heatwave extremes from an event perspective. Weather Clim. Extrem. 34, 100371.

Ma, S.M., Zhou, T.J., Stone, D.A., Angélil, O., Shiogama, H., 2017. Attribution of the July–August 2013 heat event in Central and Eastern China to anthropogenic greenhouse gas emissions. Environ. Res. Lett. 12 (5), 054020.

Min, S.-K., Kim, Y.-H., Lee, S.-M., Sparrow, S., Li, S., Lott, F.C., Stott, P.A., 2020. Quantifying human impact on the 2018 summer longest heat wave in South Korea. Bull. Am. Meteorol. Soc. 101 (1), S103–S108.

Nanding, N., Chen, Y., Wu, H., Dong, B.W., Tian, F.X., Lott, F.C., Tett, S.F.B., Rico-Ramirez, M.A., Chen, Y.H., Huang, Z.J., Yan, Y., Li, D.L., Li, R.K., Wang, X., Fan, X.W., 2020. Anthropogenic influences on 2019 july precipitation extremes over the mid–lower reaches of the yangtze river. Front. Environ. Sci. 8, 603061.

Otto, F.E.L., Massey, N., van Oldenborgh, G.J., Jones, R.G., Allen, M.R., 2012. Reconciling two approaches to attribution of the 2010 Russian heat wave. Geophys. Res. Lett. 39 (4), L04702.

Paciorek, C.J., Stone, D.A., Wehner, M.F., 2018. Quantifying statistical uncertainty in the attribution of human influence on severe weather. Weather Clim. Extrem. 20, 69–80.

Qian, C., Zhang, W.X., 2019. Short commentary on CMIP6 detection and attribution model intercomparison project (DAMIP). Clim. Chang. Res. 15 (5), 469–475 in Chinese.

Rayner, N.A., Parker, D.E., Horton, E.B., Folland, C.K., Alexander, L.V., Rowell, D.P., Kent, E.C., Kaplan, A., 2003. Global analyses of sea surface temperature, sea ice, and night marine air temperature since the late nineteenth century. J. Geophys. Res. 108 (D14), 4407.

Ren, L.W., Wang, D.Q., An, N., Ding, S.Y., Yang, K., Yu, R., Freychet, N., Tett, S.F.B., Dong, B.W., Lott, F.C., 2020. Anthropogenic influences on the persistent night-time heat wave in summer 2018 over northeast China. Bull. Am. Meteorol. Soc. 101 (1), S83–S87.

Sarojini, B.B., Stott, P.A., Black, E., 2016. Detection and attribution of human influence on regional precipitation. Nat. Clim. Change 6 (7), 669–675.

Shen, J.F., Wong, K.-y., Feng, Z.Q., 2002. State-sponsored and spontaneous urbanization in the Pearl River delta of south China, 1980-1998. Urban Geogr. 23 (7), 674–694.

Sparrow, S., Su, Q., Tian, F.X., Li, S., Chen, Y., Chen, W., Luo, F.F., Freychet, N., Lott, F.C., Dong, B.W., Tett, S.F.B., Wallom, D., 2018. Attributing human influence on the July 2017 Chinese heatwave: the influence of sea-surface temperatures. Environ. Res. Lett. 13 (11), 114004.

Stone, D.A., Pall, P., 2021. Benchmark estimate of the effect of anthropogenic emissions on the ocean surface. Int. J. Climatol. 41 (5), 3010–3026.

Sun, Y., Song, L.C., Yin, H., Zhou, B.T., Hu, T., Zhang, X.B., Stott, P., 2016. Human influence on the 2015 extreme high temperature events in western China. Bull. Am. Meteorol. Soc. 92 (12), S102–S106.

Taylor, K.E., Stouffer, R.J., Meehl, G.A., 2012. An overview of CMIP5 and the experiment design. Bull. Am. Meteorol. Soc. 93 (4), 485–498.

Trenberth, K.E., 1999. Conceptual framework for changes of extremes of the hydrological cycle with climate change. Climatic Change 42 (1), 327–339.
Utsumi, N., Seto, S., Kanae, S., Maeda, E.E., Oki, T., 2011. Does higher surface temperature intensify extreme precipitation? Geophys. Res. Lett. 38 (16), L16708.
Wang, C., Wu, K., Wu, L.G., Zhao, H.K., Cao, J., 2021. What caused the unprecedented absence of western north pacific tropical cyclones in july 2020? Geophys. Res. Lett. 48 (9), e2020GL092282.
Wang, J., Yan, Z.W., Quan, X.-W., Feng, J.M., 2016. Urban warming in the 2013 summer heat wave in eastern China. Clim. Dynam. 48 (9–10), 3015–3033.
Wang, L., Chen, W., Zhou, W., Huang, G., 2015. Understanding and detecting super-extreme droughts in Southwest China through an integrated approach and index. Q. J. R. Meteorol. Soc. 142, 529–535.
Wang, L., Yuan, X., Xie, Z., Wu, P., Li, Y., 2016. Increasing flash droughts over China during the recent global warming hiatus. Sci. Rep. 6, 30571.
Wang, Z.L., Zhong, R.D., Lai, C.G., Zeng, Z.Y., Lian, Y.Q., Bai, X.Y., 2018. Climate change enhances the severity and variability of drought in the Pearl River Basin in South China in the 21st century. Agric. For. Meteorol. 249, 149–162.
Wu, X.Y., Yang, Y., Jiang, D.B., 2023. Dramatic increase in the probability of 2006-like compound dry and hot events over Southwest China under future global warming. Weather Clim. Extrem. 41, 100592.
Xu, L.L., Zhang, T.T., Yu, W., Yang, S., 2023. Changes in concurrent precipitation and temperature extremes over the Asian monsoon region: observation and projection. Environ. Res. Lett. 18, 044021.
Xu, L.L., Yu, W., Yang, S., Zhang, T.T., 2024. Concurrent drought and heatwave events over the Asian monsoon region: insights from a statistically downscaling CMIP6 dataset. Environ. Res. Lett. 19, 034044.
Yang, T., Shao, Q.X., Hao, Z.-C., Chen, X., Zhang, Z.X., Xu, C.-Y., Sun, L.M., 2010. Regional frequency analysis and spatio-temporal pattern characterization of rainfall extremes in the Pearl River Basin, China. J. Hydrol. 380 (3–4), 386–405.
Yao, Y.L., Wang, C.Z., 2021. Variations in summer marine heatwaves in the south China sea. J. Geophys. Res.: Oceans 126 (10), e2021JC017792.
Ye, Y.B., Qian, C., 2021. Conditional attribution of climate change and atmospheric circulation contributing to the record-breaking precipitation and temperature event of summer 2020 in southern China. Environ. Res. Lett. 16 (4), 044058.
Yu, R., Zhai, P.M., 2020. More frequent and widespread persistent compound drought and heat event observed in China. Sci. Rep. 10 (1), 14576.
Yuan, X., Wang, Y.M., Ji, P., Wu, P.L., Sheffield, J., Otkin, J.A., 2023. A global transition to flash droughts under climate change. Science 380 (6641), 187–191.
Zhang, H.Y., Wu, C.H., Hu, B.X., 2019. Recent intensification of short-term concurrent hot and dry extremes over the Pearl River basin, China. Int. J. Climatol. 39 (13), 4924–4937.
Zhang, L., Zhou, T., Chen, X., Wu, P., Christidis, N., Lott, F.C., 2020. The late spring drought of 2018 in south China. Bull. Am. Meteorol. Soc. 101 (1), S59–S64.
Zhang, L.X., Chen, Z.M., Zhou, T.J., 2021. Human influence on the increasing drought risk over southeast asian monsoon region. Geophys. Res. Lett. 48 (11), e2021GL093777.
Zhang, T.T., Deng, Y., Chen, J.W., Yang, S., Dai, Y.J., 2023. An energetics tale of the 2022 mega-heatwave over central-eastern China. npj Clim. Atmos. Sci. 6, 162.
Zhao, Y.F., Zhu, J., Xu, Y., 2014. Establishment and assessment of the grid daily precipitation dataset in China in recent 50 years. J. Meteor. Sci. 34 (4), 414–420. In Chinese.
Zheng, Z.Y., Dong, W.J., Yan, D.D., Guo, Y., Wei, Z.G., Chou, J.M., Zhu, X., Wen, X.H., 2022a. Relative contributions of urbanization and greenhouse gases concentration on future climate over Beijing–Tianjin–Hebei region in China. Clim. Dynam. 58 (3–4), 1085–1105.
Zheng, Z.Y., Yan, D.D., Wen, X.H., Wei, Z.G., Chou, J.M., Guo, Y., Zhu, X., Dong, W.J., 2022b. The effect of greenhouse gases concentration and urbanization on future temperature over Guangdong-Hong Kong-Macao Greater Bay Area in China. Clim. Dynam. 58 (11–12), 3369–3392.
Zheng, Z.Y., Li, Z.C., Wen, X.H., Yan, D.D., 2024. A study of reanalysis characteristics and evaluation of interdecadal variation of the intensity of South China Sea Summer Monsoon in the early 1990s. Clim. Dynam. 1–21.
Zhou, Z.Q., Xie, S.P., Zhang, R., 2021. Historic Yangtze flooding of 2020 tied to extreme Indian Ocean conditions. Proc. Natl. Acad. Sci. USA 118 (12), e2022255118.